

21

Copy
RM SL54D05



RESEARCH MEMORANDUM

for the

U. S. Air Force

DRAG AND LONGITUDINAL TRIM CHARACTERISTICS OF A LOW-TAIL
VERSION OF THE NORTH AMERICAN YF-100A AIRPLANE AS
DETERMINED FROM THE FLIGHT TEST AT LOW LIFT
OF A 0.11-SCALE ROCKET-POWERED MODEL AT
MACH NUMBERS BETWEEN 0.75 AND 1.78

CLASSIFICATION CHANGED

By Willard S. Blanchard, Jr.

Langley Aeronautical Laboratory
Langley Field, Va.

UNCLASSIFIED

Authority of *Mason TPA 8* Effective *7-22-59*

NB 9-14-59

CLASSIFIED DOCUMENT

This material contains information affecting the National Defense of the United States within the meaning of the espionage laws, Title 18, U.S.C., Secs. 793 and 794, the transmission or revelation of which in any manner to an unauthorized person is prohibited by law.

NATIONAL ADVISORY COMMITTEE
FOR AERONAUTICS
WASHINGTON

~~CONFIDENTIAL~~

~~CONFIDENTIAL~~

NATIONAL ADVISORY COMMITTEE FOR AERONAUTICS

RESEARCH MEMORANDUM

for the

U. S. Air Force

DRAG AND LONGITUDINAL TRIM CHARACTERISTICS OF A LOW-TAIL
VERSION OF THE NORTH AMERICAN YF-100A AIRPLANE AS
DETERMINED FROM THE FLIGHT TEST AT LOW LIFT
OF A 0.11-SCALE ROCKET-POWERED MODEL AT
MACH NUMBERS BETWEEN 0.75 AND 1.78

By Willard S. Blanchard, Jr.

SUMMARY

Drag and longitudinal trim characteristics at low lift of a low-tail version of the North American YF-100A airplane as obtained from the flight test of a 0.11-scale rocket model at Mach numbers from 0.75 to 1.78 are presented herein. Also included are some longitudinal stability data and some qualitative damping-in-pitch data.

The subsonic external drag level was 0.012. The drag rise, based on $dC_D/dM = 0.10$, began at $M = 0.93$. The drag coefficient peaked at a value of 0.039 at $M \approx 1.10$ and decreased to a value of 0.034 at $M = 1.71$. The low-lift longitudinal trim change was mild and consisted of a nosing-up tendency between subsonic speeds and $M = 1.30$. It should be noted that the model had its center of gravity approximately 10 percent mean aerodynamic chord ahead of the full-scale airplane center of gravity. Damping in pitch appeared to decrease at the lower supersonic speeds. There was no indication of tail buffet or flutter during any portion of the test reported herein.

INTRODUCTION

An investigation at low lift of the drag and longitudinal trim characteristics of 0.11-scale rocket models of the North American YF-100A has been conducted by the Langley Pilotless Aircraft Research Division at the request of the U. S. Air Force.

~~CONFIDENTIAL~~

The YF-100A is a swept-wing jet-propelled fighter-type airplane of conventional configuration with nose inlet, and is designed to fly at supersonic speeds. The primary purpose of the test reported herein was to obtain drag and longitudinal trim data for the clean configuration of a low-tail version of the airplane. This model was a modification of the model of reference 1, which had a thicker, higher horizontal tail, a thicker vertical tail, a larger canopy, and a longer fuselage. In addition to drag and trim data, however, some longitudinal stability and pitch-damping data were obtained through analyses of pitch disturbances created by sustainer motor burnout and by two pulse rockets.

SYMBOLS

M	free-stream Mach number
R	Reynolds number based on mean aerodynamic chord
W	model weight, 139.7 lb
\bar{c}	mean aerodynamic chord
q	free-stream dynamic pressure, lb/sq ft
S	model wing area (leading and trailing edges extended to fuselage center line), 4.56 sq ft
C_C	chord-force coefficient, $\frac{\text{Chord force}}{qS}$
C_D	drag coefficient, $\frac{\text{Drag}}{qS}$
ΔC_D	pressure drag coefficient
dC_D/dM	rate of change of drag coefficient with Mach number
C_N	normal-force coefficient, $\frac{\text{Normal force}}{qS}$
C_L	lift coefficient, $\frac{\text{Lift}}{qS}$
C_m	pitching-moment coefficient about the center of gravity, $\frac{\text{Pitching moment}}{qS\bar{c}}$
α	angle of attack, deg

$C_{m\alpha}$	rate of change of pitching-moment coefficient with angle of attack, $\frac{dC_m}{d\alpha}$, per deg
P	period of the short-period longitudinal oscillation, sec
q	$\frac{d\theta}{dt}$, radians/sec
$\dot{\alpha}$	$\frac{d\alpha}{dt}$, radians/sec
$C_{L\alpha}$	rate of change of lift coefficient with angle of attack, $dC_L/d\alpha$, per deg
V	velocity, ft/sec
t	time, sec
γ	flight-path angle
C_{mq}	$\frac{\partial C_m}{\partial \left(\frac{qc}{2V}\right)}$, per radian
$C_{m\dot{\alpha}}$	$\frac{\partial C_m}{\partial \left(\frac{\dot{\alpha}c}{2V}\right)}$, per radian
A	cross-sectional area or aspect ratio
l	model length from nose to fuselage base
x	distance measured rearward from nose, ft
r	radius, ft
a_l/g	longitudinal-accelerometer reading
a_n/g	normal-accelerometer reading
$T_{1/2}$	time required for the short-period longitudinal oscillation to damp to one-half amplitude, sec

MODEL

Figure 1 is a three-view drawing of the model used in this investigation. Figure 2 shows cross-sectional area of the components plotted nondimensionally against fuselage station, and figure 3 shows total cross-sectional area for the model of this test and the model of reference 1 plotted dimensionally against fuselage station. Figures 4 to 6 are photographs of the model. Table I includes geometric dimensions of the model tested and of the model of reference 1.

The model had no duct inlet; the fuselage lines were faired to a pointed nose ahead of the inlet location. The fuselage was built around a $5\frac{1}{2}$ -inch-diameter steel tube which served to house the sustainer rocket motor and to secure the wing, nose, and tail. The fuselage was of mahogany with the exception of the nose, which was of fiber glass with heat-resistant plastic used as a bonding agent. The wing was 7 percent thick and was solid aluminum. The horizontal and vertical tails were $3\frac{1}{2}$ percent thick and were solid steel.

The sustainer motor was a solid-fuel rocket motor developing about 3,700 pounds of thrust for 1 second, and served to accelerate the model from $M = 1.25$ to $M = 1.78$. The model was equipped with two small pulse rockets which were used to disturb the model in pitch at preset times during the flight in order to obtain the stability data presented herein. These pulse rockets were located on the bottom of the fuselage near the tail.

Instrumentation consisted of a four-channel telemeter which transmitted continuous records of free-stream total pressure, normal acceleration, longitudinal acceleration, and horizontal-tail normal acceleration.

The wing and horizontal tail were mounted at zero degrees incidence with respect to the model reference line. The center of gravity was located 20.6 percent behind the leading edge of the mean aerodynamic chord.

TEST PROCEDURE

The model was boosted to $M = 1.30$ by a solid-fuel Deacon rocket motor developing an average thrust of about 6,000 pounds for 3 seconds. Data transmitted by the telemeter were recorded by two independent ground receiving stations. Throughout the flight, the model was tracked by two radar sets, one recording position in space and the other recording radial velocity.

A radiosonde was used to determine atmospheric density, pressure, and temperature throughout the altitude range traversed by the model flight.

METHOD OF ANALYSIS

All data reported herein were obtained from the decelerating portion of the model flight where the model was separated from the booster and the sustainer rocket was not thrusting. Dynamic pressure and Mach number were determined from telemetered total pressure and radiosonde static pressure.

Drag

Total drag was determined by two independent methods. The first consisted of differentiation with respect to time of the velocity (as determined from radar tracking, and corrected for flight-path angle) and calculation of total-drag coefficient by the relationship

$$C_{D_{total}} = - \left(\frac{dV}{dt} + 32.2 \sin \gamma \right) \frac{W}{32.2qS}$$

The second method consisted of calculating drag coefficient by the relationship

$$C_{D_{total}} = C_c = - \left(\frac{a_1}{g} \right) \left(\frac{W}{qS} \right)$$

where a_1/g was determined directly from telemetered data and $C_{D_{total}}$ was assumed equal to C_c since the model flew near zero lift.

External drag was calculated from the relationship

$$C_{D_{external}} = C_{D_{total}} - C_{D_{base}}$$

where $C_{D_{base}}$ was determined using the same base pressure coefficient as the model of reference 1.

Lift

Lift was determined from the relationship

$$C_L = C_N = \left(\frac{a_n}{g}\right)\left(\frac{W}{qS}\right)$$

where a_n/g was determined directly from telemetered data, and C_L was assumed equal to C_N since the model flew near zero lift. Static longitudinal stability and damping in pitch were calculated by the methods used in reference 2.

DISCUSSION OF RESULTS

Reynolds number varied from 4.6×10^6 at $M = 0.75$ to 14.2×10^6 at $M = 1.78$ as shown in figure 7. The center of gravity was located 20.6 percent behind the leading edge of the mean aerodynamic chord. The center of gravity of the model of reference 1 was at 19.6 percent mean aerodynamic chord.

Longitudinal Trim

Low-lift longitudinal trim is shown in figure 8 for this test and for the model of reference 1. The longitudinal trim change was small and consisted of a nosing-up tendency between subsonic speeds and $M = 1.30$. It should be noted that the model center-of-gravity location was farther forward than for the full-scale airplane (0.20 \bar{c} compared to about 0.30 \bar{c}).

Drag

External drag, as determined from figures 9 and 10, is presented in figure 11 along with external drag from reference 1. The subsonic external drag level is about 0.012. The drag rise, based on $dC_D/dM = 0.10$, occurs at $M = 0.93$. The peak drag coefficient is 0.039 and occurs at $M \approx 1.10$. Between $M = 1.10$ and $M = 1.71$, the external drag coefficient decreases from 0.039 to 0.034. The referenced values are from a rocket model test of an earlier version of the same airplane, employing a thicker tail (7 percent), a larger canopy, and a slightly shorter fuselage. The effects of these differences in configuration on the area distribution can be seen in figure 3. Comparison of the two curves shown in figure 11 indicates that the later version, reported

herein, has slightly higher subsonic drag, a less-abrupt drag rise, and appreciably less drag at speeds above $M = 1.0$. The lower drag at supersonic speeds is felt to be the effect of the less blunt body resulting from the smaller canopy and the thinner horizontal and vertical tails.

Variation of pressure drag with Mach number is shown in figure 12. Comparison between the test results of reference 1 and values from reference 3, which are from a body-of-revolution model having the same area distribution as the model of reference 1, indicates that the transonic area rule does not accurately predict the peak pressure drag of a configuration of this type. Further, results from the test reported herein and the test of reference 1, as compared to values of peak pressure drag for corresponding bodies of revolution, calculated by the method of reference 4, leads to the same conclusion. It is interesting to note, however, that the increment between the measured drags of the configurations agrees well with the calculated increments between the corresponding bodies of revolution, at $M = 1.2$.

Longitudinal Stability

The period of the short-period pitch oscillation is shown in figure 13. Figure 14 shows the static-longitudinal-stability parameter $C_{m\alpha}$ as determined from the values of pitch period presented in figure 13. Figure 14 shows a gentle decrease in $C_{m\alpha}$ from about -0.034 at $M = 1.25$ to about -0.020 at $M = 1.75$.

Lift-curve slope, as determined from references 5 and 6 and corrected for the flexibility of this model, is shown in figure 15. These values were used to calculate the stability data in this paper. Figure 16 shows aerodynamic-center location from the present test, and from reference 1. While the variation with Mach number is similar for the model of this test and the model reported in reference 1, the model of this test has its aerodynamic center located about 10 percent farther rearward than the model of reference 1. This is caused at least partially by the greater stiffness of the horizontal tail of the model of this test, and probably is somewhat affected by the vertical location of the horizontal tail (the horizontal tail of the model of this test was located below the wing chord plane, while on the model of reference 1 the horizontal tail was above the wing chord plane).

Damping in Pitch

Time required for the short period longitudinal oscillation to damp to one-half amplitude is shown in figure 17. Figure 18 shows values

of $C_{m_q} + C_{m_{\dot{\alpha}}}$ as determined using the values of $T_{1/2}$ shown in figure 17. Also shown are values from reference 1, and values calculated by the method of reference 7, using values of downwash from reference 8. At the higher supersonic speeds, damping measured in both the test reported herein and the test of reference 1 is higher than the values calculated by the method of reference 7. At the lower supersonic speeds, however, the measured damping appears to decrease appreciably below the calculated values.

Flutter and Buffet

As noted in the description of the model, a normal accelerometer was installed in the tail. This accelerometer showed no indication of tail buffet or flutter during any portion of the test reported herein.

CONCLUSIONS

From the test of a 0.11-scale rocket model of a low-tail version of the North American YF-100A airplane at Mach numbers between 0.75 and 1.78 at low lift, the following conclusions are indicated:

1. The subsonic level of the external drag coefficient was 0.012, the drag rise based on $dC_D/dM = 0.10$ began at $M = 0.93$, the drag coefficient peaked at a value of 0.039 at $M \approx 1.10$ and then decreased to a value of 0.034 at $M = 1.71$.
2. The low-lift longitudinal trim change was mild and consisted of a nosing-up tendency between subsonic speeds and $M = 1.30$. It should be noted that the model center of gravity was approximately 10 percent mean aerodynamic chord farther forward than that of the full-scale airplane.
3. Damping in pitch appeared to decrease at the lower supersonic speeds.

4. There was no indication of tail buffet or flutter during any portion of the test reported herein.

Langley Aeronautical Laboratory,
National Advisory Committee for Aeronautics,
Langley Field, Va., March 16, 1954.

Willard S. Blanchard, Jr.

Willard S. Blanchard, Jr.
Aeronautical Research Scientist

Approved:

Joseph A. Shortal
Joseph A. Shortal
Chief of Pilotless Aircraft Research Division

MML

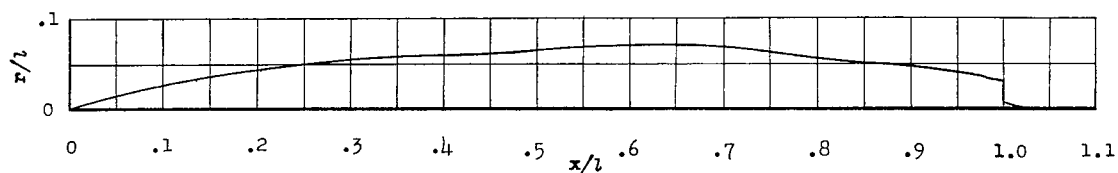
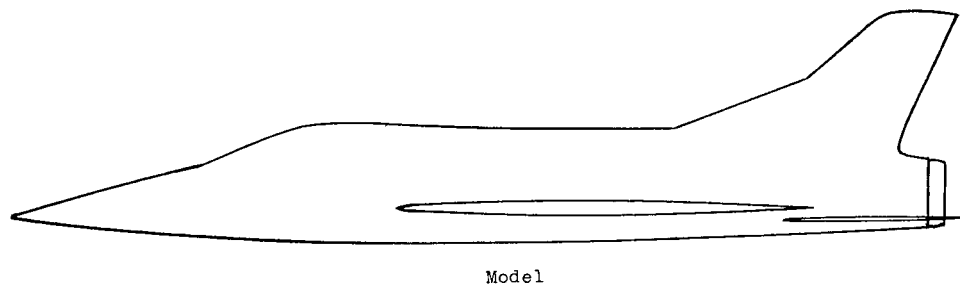
REFERENCES

1. Blanchard, Willard S., Jr.: A Summary of the Drag and Longitudinal Trim at Low Lift of the North American YF-100A Airplane at Mach Numbers From 0.75 to 1.77 As Determined by Flight Tests of 0.11-Scale Rocket Models. NACA RM SL54B01, U. S. Air Force, 1954.
2. Gillis, Clarence L., Peck, Robert F., and Vitale, A. James: Preliminary Results From a Free-Flight Investigation at Transonic and Supersonic Speeds of the Longitudinal Stability and Control Characteristics of an Airplane Configuration With a Thin Straight Wing of Aspect Ratio 3. NACA RM L9K25a, 1950.
3. Hall, James Rudyard: Comparison of Free-Flight Measurements of the Zero-Lift Drag Rise of Six Airplane Configurations and Their Equivalent Bodies of Revolution at Transonic Speeds. NACA RM L53J21a, 1954.
4. Nelson, Robert L., and Stoney, William E., Jr.: Pressure Drag of Bodies at Mach Numbers up to 2.0. NACA RM L53I22c, 1953.
5. Mardin, H. R.: Supersonic Wind Tunnel Tests of the 0.02 Scale Full Span Model of the NA-180 (YF-100A) Airplane Through a Mach Number Range of 0.70 to 2.87 To Determine the Effect of Modifications to the Basic Model Components on the Aerodynamic Characteristics. Rep. No. SAL-43, North American Aviation, Inc., Oct. 30, 1952.
6. Safier, Irving: Report on Wind Tunnel Tests of a 0.07-Scale Sting-Mounted Model of the North American (Inglewood) F-100A (NA-180) Airplane at High Subsonic Speeds and $M = 1.20$. CWT Rep. 258, Southern Calif. Cooperative Wind Tunnel, Sept. 4, 1952.
7. Gillis, Clarence L., and Chapman, Rowe, Jr.: Summary of Pitch-Damping Derivatives of Complete Airplane and Missile Configurations As Measured in Flight at Transonic and Supersonic Speeds. NACA RM L52K20, 1953.
8. Weil, Joseph, Campbell, George S., and Diederich, Margaret S.: An Analysis of Estimated and Experimental Transonic Downwash Characteristics As Affected by Plan Form and Thickness for Wing and Wing-Fuselage Configurations. NACA RM L52I22, 1952.

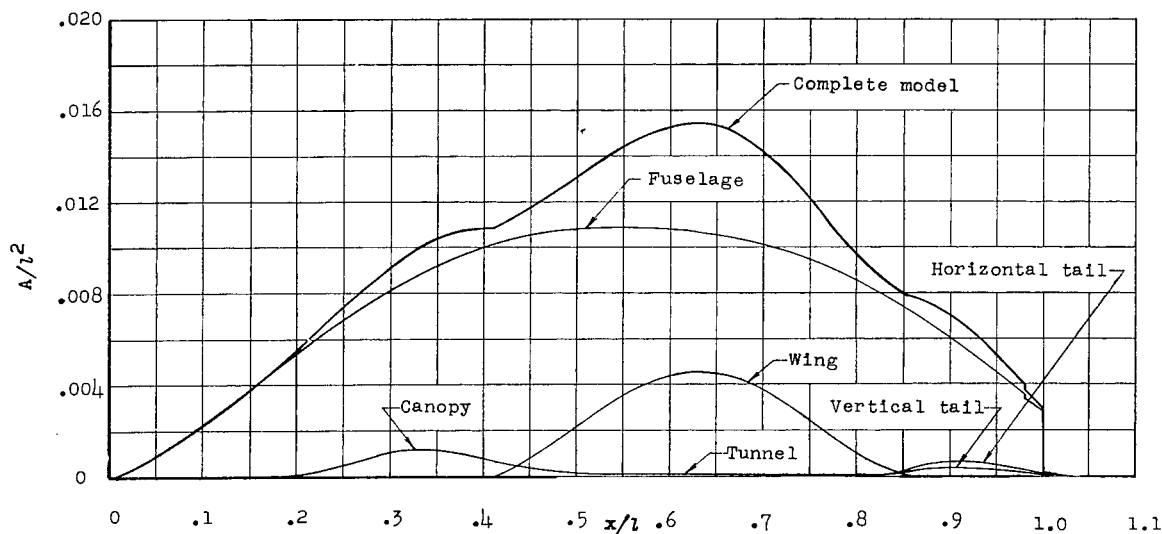
TABLE I.- GEOMETRIC DIMENSIONS

	Model of ref. 1 (High tail)	Present test (Low tail)
Wing:		
Total area, sq ft	4.56	4.56
Exposed area, sq ft	3.54	3.54
Aspect ratio	3.56	3.56
Sweepback (quarter chord), deg . . .	45	45
Taper ratio	0.30	0.30
Horizontal tail:		
Total area, sq ft	1.20	1.20
Exposed area, sq ft	0.85	0.85
Aspect ratio	3.56	3.56
Sweepback (quarter chord), deg . . .	45	45
Taper ratio	0.30	0.30
Vertical tail:		
Total area (to center line), sq ft .	0.60	0.69
Exposed area, sq ft	0.46	0.54
Aspect ratio	1.76	1.45
Sweepback (quarter chord), deg . . .	45	45
Taper ratio	0.28	0.41
Fuselage:		
Frontal area, sq ft	0.32	0.32
Length, ft	*5.25	*5.47
Base area, sq ft	0.054	0.084
Fuselage nose to wing leading edge (center line), ft	*1.725	*1.90
Fuselage nose to horizontal-tail leading edge (center line), ft . . .	*4.135	*4.14
Wing chord plane to fuselage reference line, ft	0.104	0.104
Tail chord plane to fuselage reference line, ft	0.058	0.161
Wing airfoil section, free stream . . .	NACA 64A007	
Horizontal- and vertical-tail airfoil sections, free stream	NACA 64A007	NACA 64A003.5

*Includes faired nose (no inlet).



(a) Equivalent body of revolution (complete model).



(b) Breakdown of areas of the components.

Figure 2.- Nondimensional area distribution of the model tested.

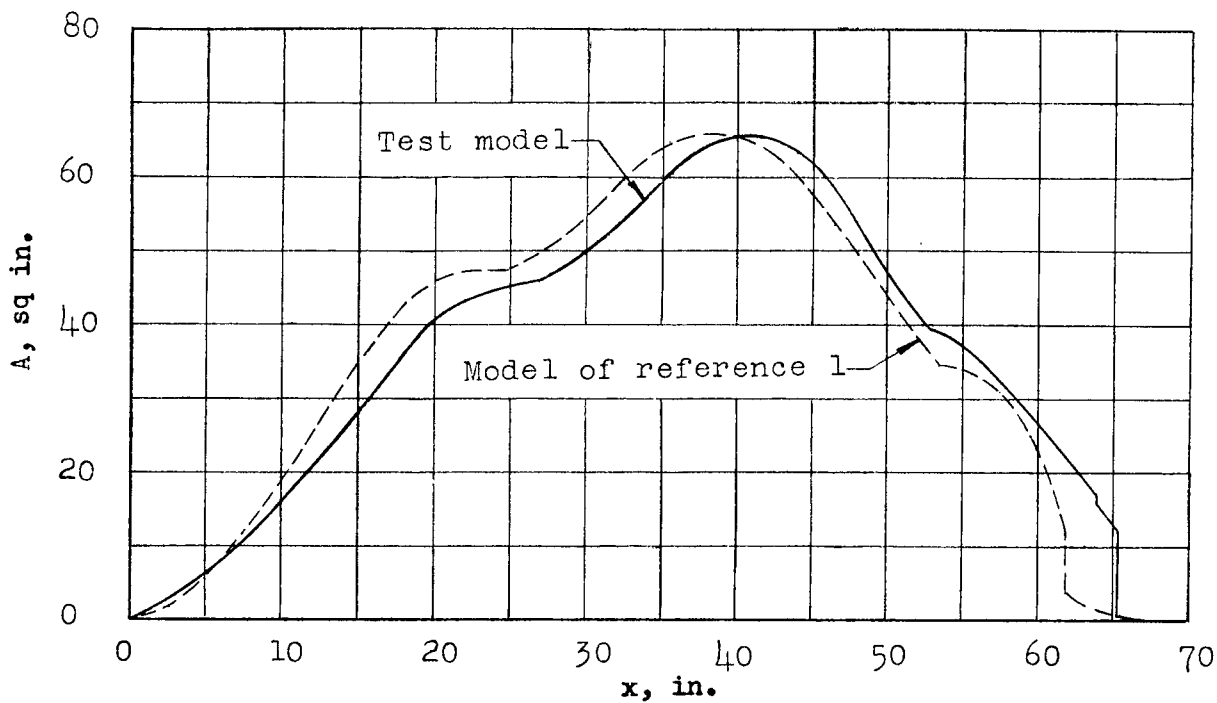
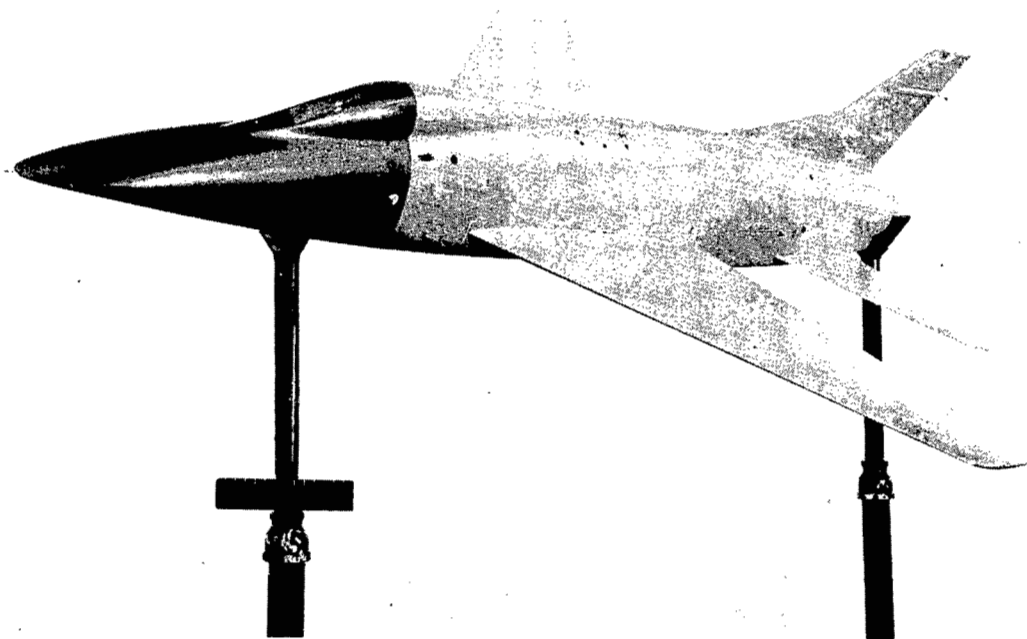


Figure 3.- Dimensional area distribution.



L-80907.1

Figure 4.- Three-quarter front view of the model tested.

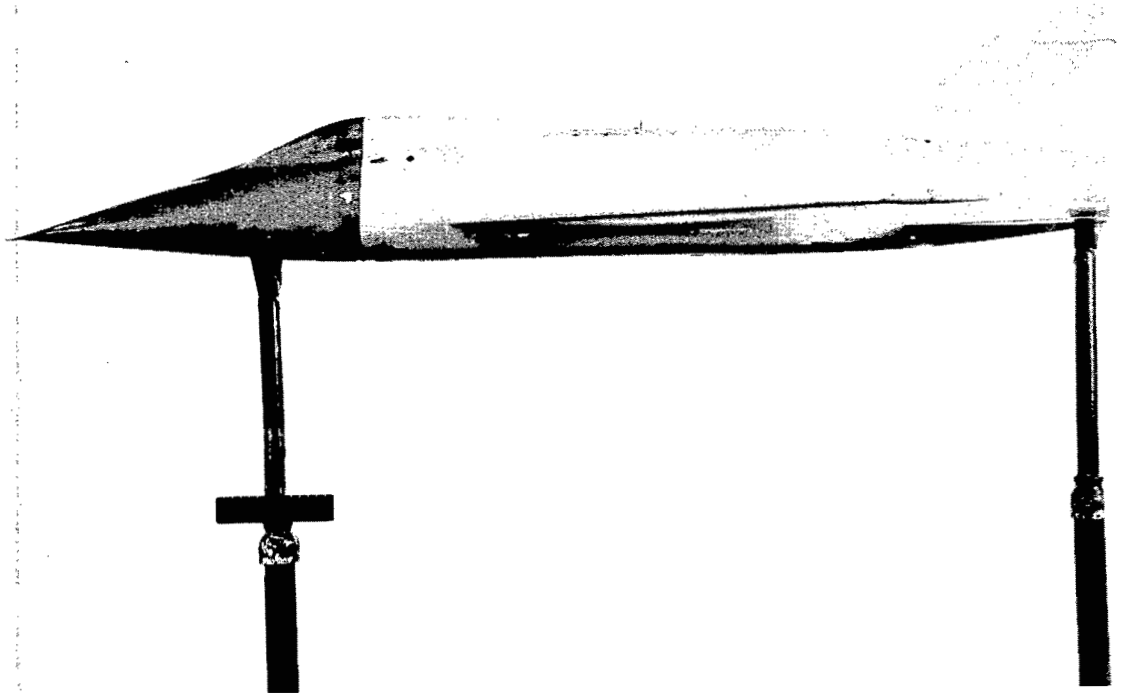
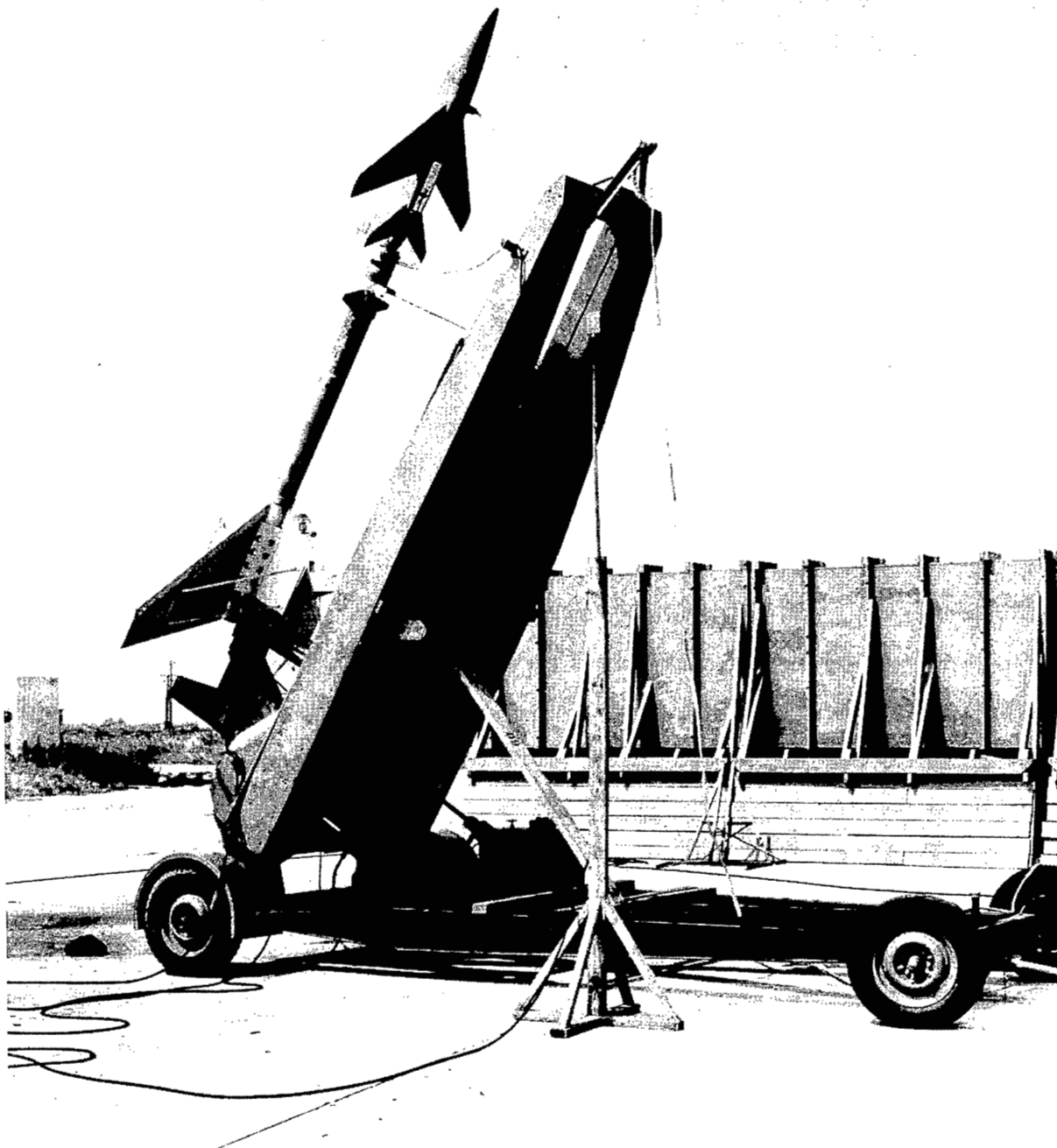


Figure 5.- Side view of the model tested.

L-80905.1



L-81058.1

Figure 6.- The model-booster combination in launching position.

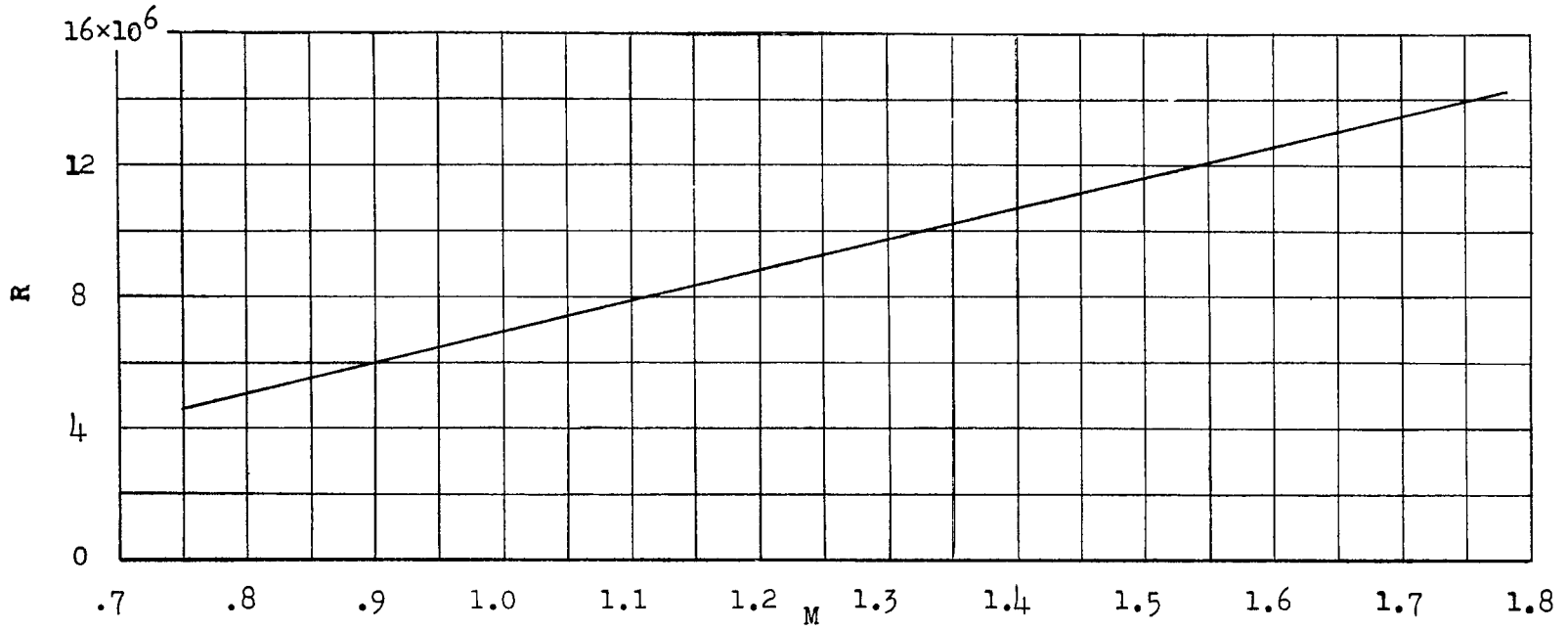


Figure 7.- Variation of Reynolds number with Mach number.

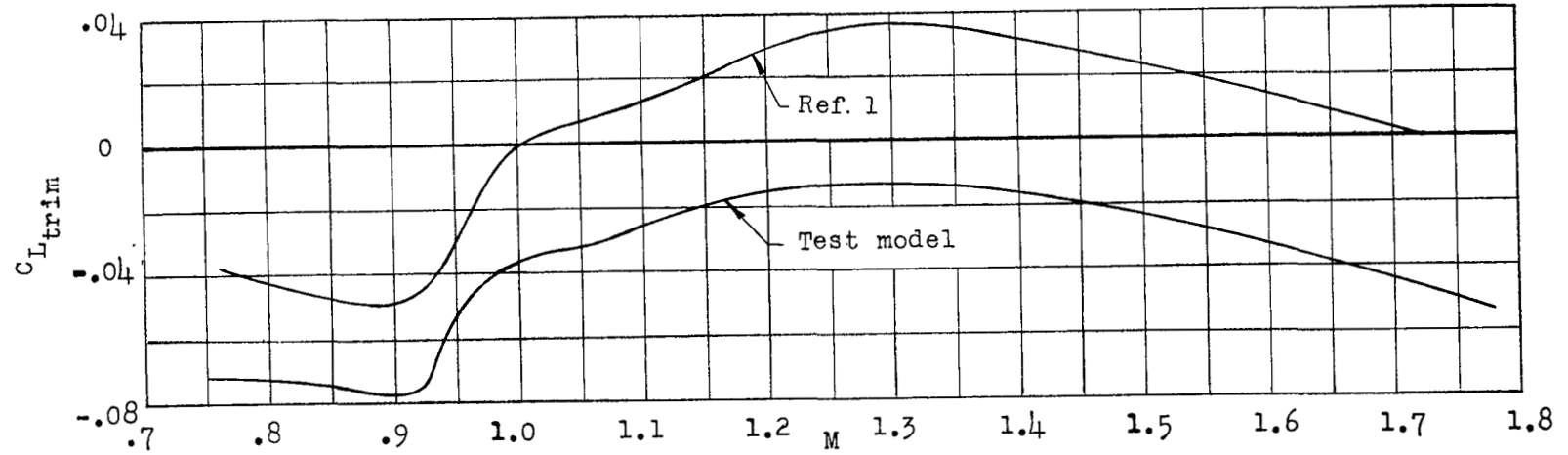


Figure 8.- Longitudinal trim.

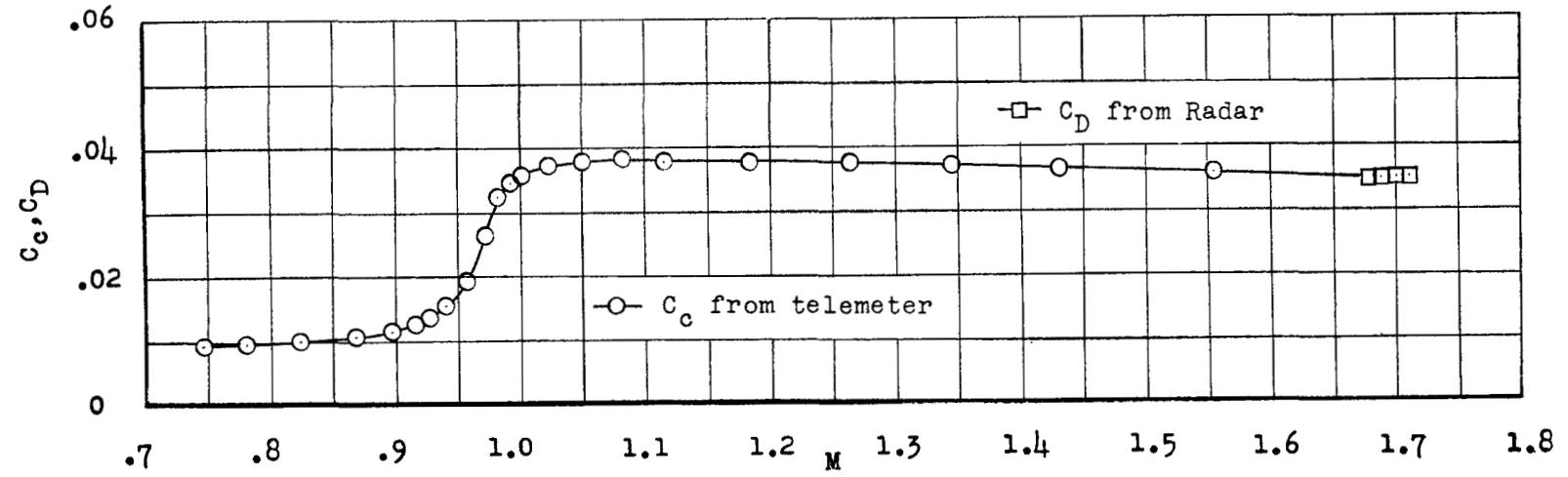


Figure 9.- Total drag and chord force.

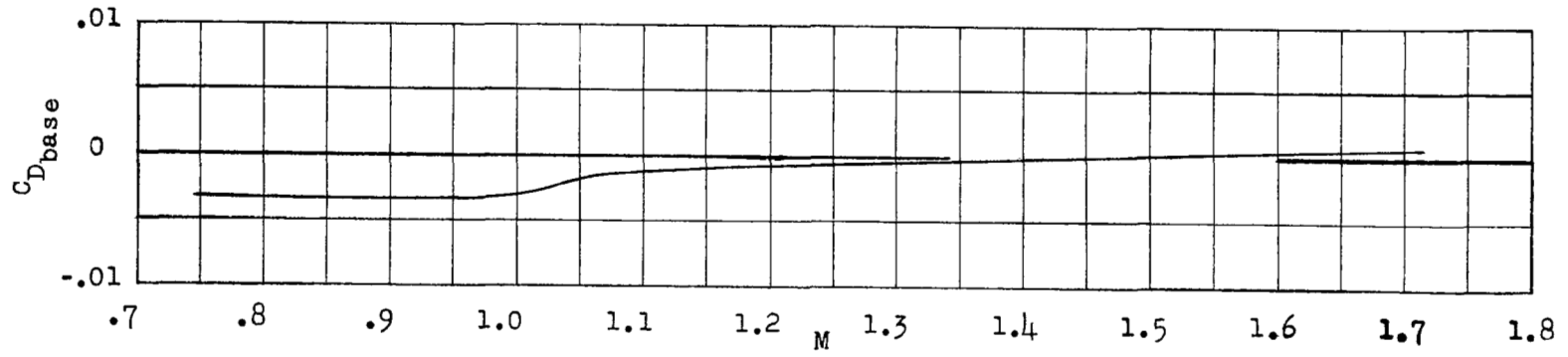


Figure 10.- Base drag (ref. 1).

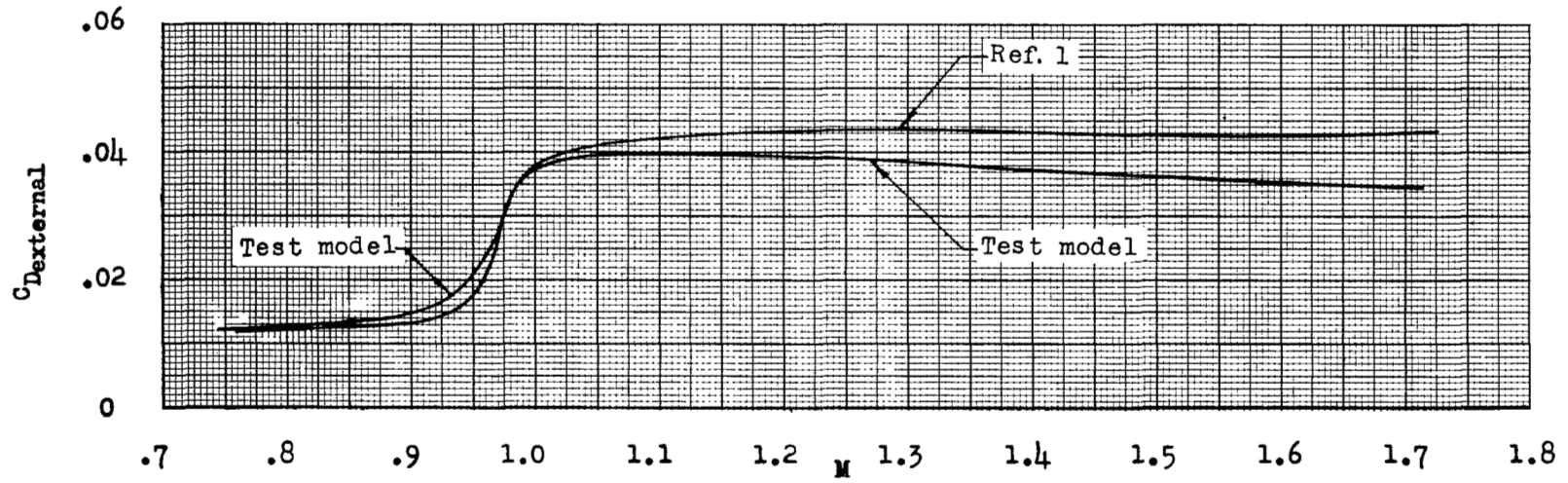


Figure 11.- External drag.

CONFIDENTIAL

CONFIDENTIAL

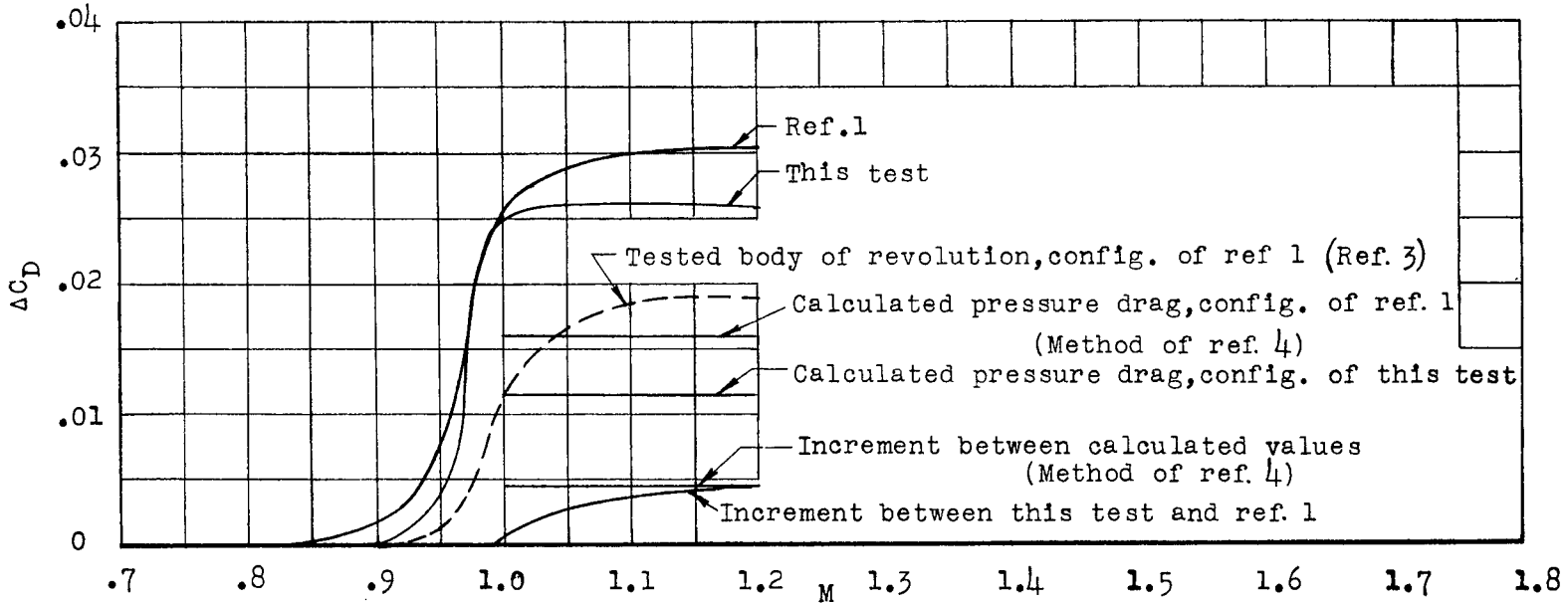


Figure 12.- Pressure drag.

CONFIDENTIAL

CONFIDENTIAL

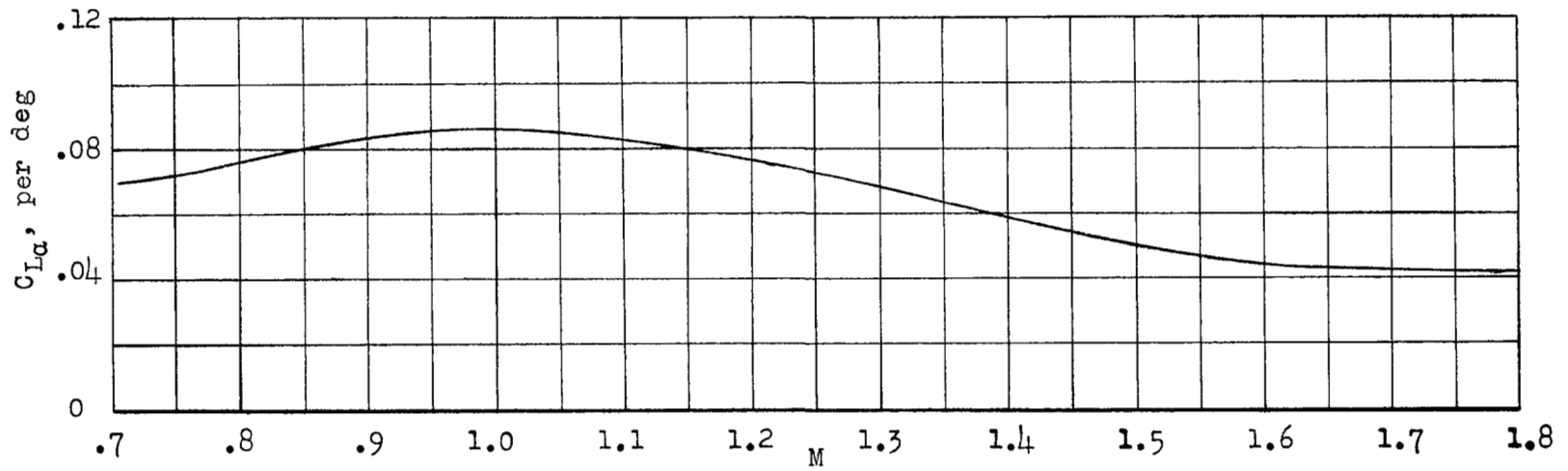


Figure 15.- Calculated lift-curve slope, including corrections for flexibility of the model tested.

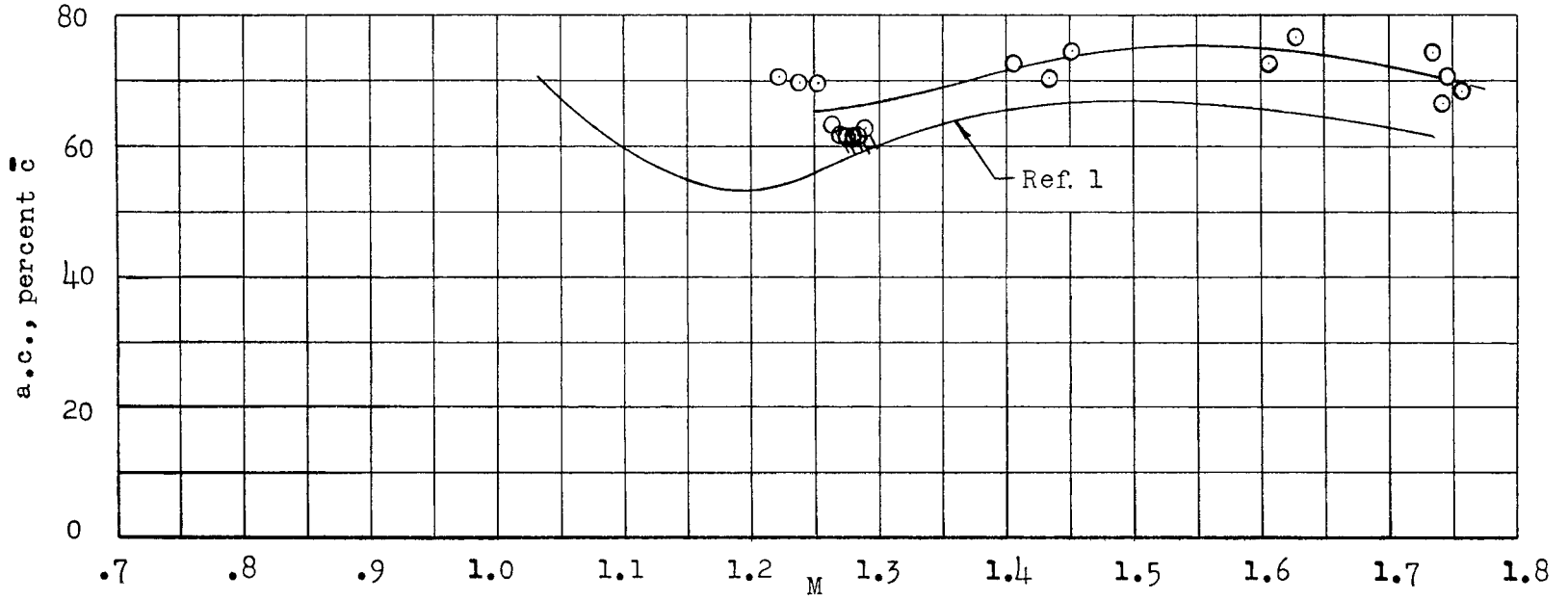


Figure 16.- Aerodynamic-center location. Tailed symbols indicate data obtained between booster motor burnout and sustainer firing.

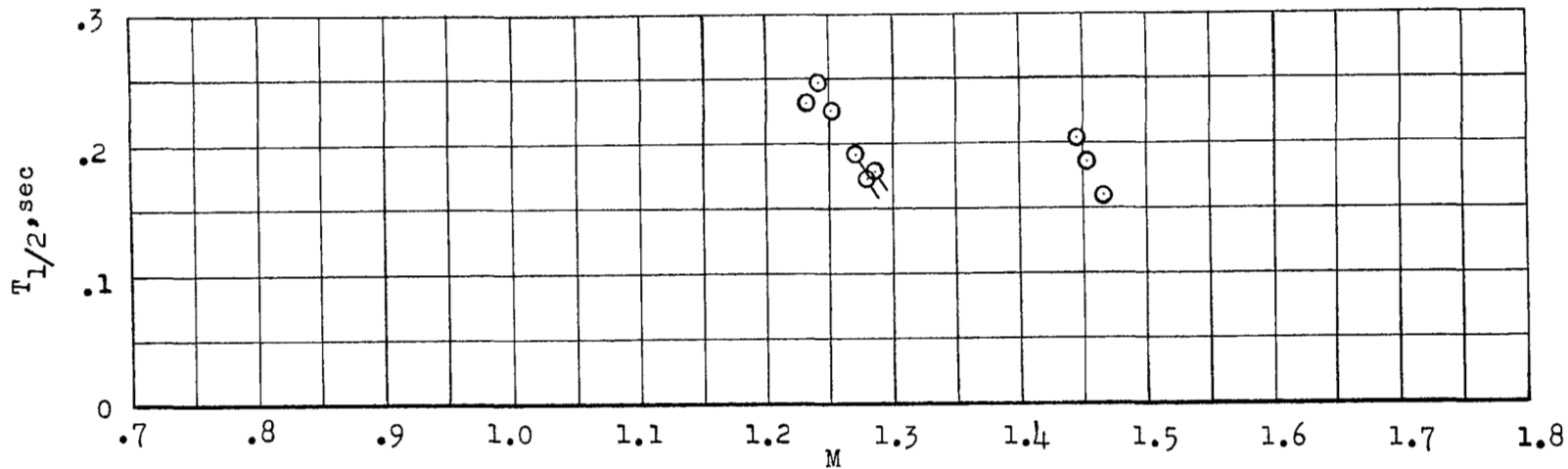


Figure 17.- Time required for the short-period longitudinal oscillation to damp to one-half amplitude. Tailed symbols indicate data obtained between booster motor burnout and sustainer firing.

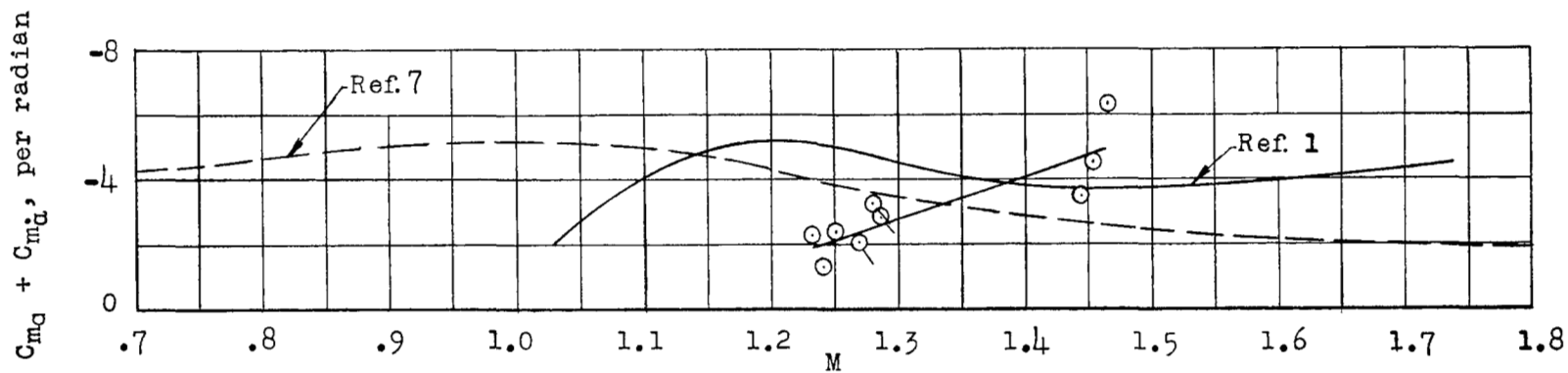


Figure 18.- Damping in pitch.